FERMILAB-PUB-08-411-CD

Discovery of A Very Bright, Strongly-Lensed $z = 2$ Galaxy in the SDSS DR5

Huan Lin[1], Elizabeth Buckley-Geer[1], Sahar S. Allam[1,2], Douglas L. Tucker[1], H. Thomas Diehl[1], Donna Kubik[1], Jeffrey M. Kubo[1], James Annis[1], Joshua A. Frieman[1,3], Masamune Oguri[4], Naohisa Inada[5]

ABSTRACT

We report on the discovery of a very bright $z = 2.00$ star-forming galaxy that is strongly lensed by a foreground $z = 0.422$ luminous red galaxy (LRG). This system was found in a systematic search for bright arcs lensed by LRGs and brightest cluster galaxies in the Sloan Digital Sky Survey Data Release 5 sample. Follow-up observations on the Subaru 8.2m telescope on Mauna Kea and the Astrophysical Research Consortium 3.5m telescope at Apache Point Observatory confirmed the lensing nature of this system. A simple lens model for the system, assuming a singular isothermal ellipsoid mass distribution, yields an Einstein radius of $\theta_{\rm Ein} = 3.82 \pm 0.03''$ or $14.8 \pm 0.1 h^{-1}$ kpc at the lens redshift. The total projected mass enclosed within the Einstein radius is $2.10 \pm 0.03 \times 10^{12} h^{-1} M_\odot$, and the magnification factor for the source galaxy is 27 ± 1. Combining the lens model with our $gVriz$ photometry, we find an (unlensed) star formation rate for the source galaxy of 32 h^{-1} $M_\odot$ yr^{-1}, adopting a fiducial constant star formation rate model with an age of 100 Myr and $E(B-V) = 0.25$. With an apparent magnitude of $r = 19.9$, this system is among the very brightest lensed $z \geq 2$ galaxies, and provides an excellent opportunity to pursue detailed studies of the physical properties of an individual high-redshift star-forming galaxy.

Subject headings: gravitational lensing — galaxies: high-redshift

---

[1]Fermi National Accelerator Laboratory, P.O. Box 500, Batavia, IL 60510

[2]University of Wyoming, Dept. of Physics & Astronomy, P.O.Box 3905, Laramie, WY 82071

[3]Kavli Institute for Cosmological Physics and Department of Astronomy and Astrophysics, University of Chicago, 5640 South Ellis Avenue, Chicago, IL 60637

[4]Kavli Institute for Particle Astrophysics and Cosmology, Stanford University, 2575 Sand Hill Road, Menlo Park, CA 94025

[5]Cosmic Radiation Laboratory, RIKEN, 2-1 Hirosawa, Wako, Saitama 351-0198, Japan

1. Introduction

Strong lensing systems provide the dual opportunity to study both the foreground mass distribution along the line of sight to the lens and the physical properties of the background object that is being lensed. The latter is especially useful in studies of high-redshift galaxies, for which lensing provides a vital boost in the apparent brightness of these faint objects, which are otherwise difficult to study in detail.

For many years the $z = 2.72$ system cB58 (Yee et al. 1996) served as the prototypical lensed high-redshift Lyman break galaxy (LBG; e.g., Steidel et al. 2003). At $r = 20.4$, it is very bright and thereby allowed a number of detailed studies of the physical properties of a *single* LBG to be carried out (e.g., Pettini et al. 2000; Teplitz et al. 2000). Recently a number of high-redshift lensed systems have been discovered, either serendipitously or in systematic searches, that are brighter than cB58 (Smail et al. 2007; Belokurov et al. 2007), including the current record holder, the "8 o'clock arc," at $r = 19.2$ (Allam et al. 2007). These discoveries have been enabled by the Sloan Digital Sky Survey (SDSS; York et al. 2000), which provides the very large search area needed to systematically find these rare examples of extremely bright lensed high-redshift galaxies.

In this paper we report on the discovery of another remarkably bright ($r = 19.9$) strongly lensed $z = 2.00$ galaxy, the first system we have confirmed from a systematic search program for very bright lensed arcs that we are carrying out using the SDSS data. This paper is organized as follows: §2 describes the arc search and the discovery, §3 describes the follow-up imaging and spectroscopy that led to confirmation of the system as a gravitational lens, §4 describes the modeling of the system including the photometry measurements, § 5 describes the source galaxy star formation rate measurements, and finally §6 presents our conclusions. We assume a flat cosmology with $\Omega_M = 0.3$, $\Omega_\Lambda = 0.7$, and $H_0 = 100h$ km s^{-1} Mpc^{-1}, unless otherwise noted.

2. Arc Search Sample

The SDSS (York et al. 2000) is a digital imaging and spectroscopic survey that, over the course of five years, mapped nearly one quarter of the celestial sphere in five filter bands (*ugriz*; Fukugita et al. 1996) down to $r = 22.2$ and obtained spectra for $\approx 10^6$ astronomical objects (Adelman-McCarthy et al. 2007). The SDSS completed its first phase of operations in June 2005 and recently completed a three-year extension known as SDSS-II in July 2008. (For more details, please consult `www.sdss.org`.)

We previously reported the serendipitous discovery in the SDSS Data Release 4 (DR4;

Adelman-McCarthy et al. 2006) of the brightest lensed Lyman break galaxy (LBG) currently known, the 8 o'clock arc (Allam et al. 2007). The LBG in that system is at a redshift of 2.73 and is lensed by a luminous red galaxy (LRG) at a redshift of 0.38. The three bright gravitationally lensed images have a total magnitude of $r = 19.2$ and are quite blue ($g - r = 0.7$). Motivated by this discovery and using the characteristics of the 8 o'clock arc system as our starting point, we have conducted a systematic search (Kubik 2007)[1] for similar systems in the SDSS Data Release 5 (DR5; Adelman-McCarthy et al. 2007). The search started from two catalogs: the first consisting of 221,000 LRGs derived from the SDSS database and the second consisting of 29,000 brightest cluster galaxies (BCGs) compiled by one of us (J. Annis) using an earlier version (Hansen et al. 2005) of the maxBCG cluster finding technique (Koester et al. 2007). We defined a database query which was run on the DR5 Catalog Archive Server (CAS) database. This query searched for LRGs and BCGs which have one or more neighboring blue objects, defined using color cuts $g - r < 1$ and $r - i < 1$, that were detected by the SDSS photometric pipeline within a search radius of $10''$. We note that due to issues of seeing and object deblending in the SDSS, our search will effectively find systems with Einstein radii larger than about $2''$ or so. Our search is therefore complementary to a spectroscopic lensing survey like the Sloan Lens ACS Survey (SLACS; Bolton et al. 2006), which is limited to systems with image separations smaller than the $3''$ SDSS spectroscopic fiber diameter.

Our query returned 57,485 systems, which were then ranked by the number of blue objects, n. The 1081 systems with $n \geq 3$ were inspected by four separate inspectors who looked for arc-like morphology in the SDSS CAS gri color jpeg images. The 14 final candidates found in this sample have already been described in Kubik (2007), including an initial analysis of their Einstein radii and mass-to-light ratios. To date we have spectroscopically confirmed 6 of them as lensed, including 3 with source redshifts $z \geq 2$. Additional details of follow-up observations and lens modeling for these systems, as well as for other systems found in a separate search of a sample of SDSS interacting/merging galaxies, will be the subject of future papers. One inspector also examined the 7442 systems in the $n = 2$ sample, which yielded the object described in this paper. This system was the brightest and most striking arc candidate from the $n = 2$ list, and we dubbed the system the "Clone" as it was very similar to the 8 o'clock arc in morphology and brightness. In Fig. 1 we show the discovery SDSS image of this system. The lensing LRG is the object SDSS J120602.09+514229.5, and Fig. 2 shows its SDSS spectrum, indicating absorption features of an early type elliptical galaxy at a redshift of 0.422. The very blue arc knots, labeled A1 through A3 in Fig. 1, are associated with two objects identified by the SDSS photometric pipeline (A1/A2 = SDSS

[1]http://www.physics.niu.edu/physics/academic/grad/theses/Donna.pdf

J120601.69+514227.8 and A3 = SDSS J120601.93+514233.5), but they are not SDSS spectroscopic targets and so do not have any SDSS spectroscopic redshifts.

3. Follow-up Imaging and Spectroscopy

In order to confirm the Clone system as a gravitational lens we have carried out a follow-up program of imaging and spectroscopy using the Astrophysical Research Consortium (ARC) 3.5m telescope at Apache Point Observatory (APO) and the 8.2m Subaru telescope on Mauna Kea.

3.1. Subaru Imaging and Spectroscopy

Initial follow-up imaging and long-slit spectroscopy were carried out with the Faint Object Camera and Spectrograph (FOCAS) instrument on the Subaru 8.2m telescope (Kashikawa et al. 2002); see the observation log in Table 1. The instrument has a $6'$ circular field of view and the pixel scale is $0.208''$ per pixel (when binned by 2×2).

Three 15-sec V-band exposures were taken using the FOCAS instrument, under good seeing conditions of $0.53''$ FWHM as measured from stars in the images. The images were bias subtracted and flatfielded using standard routines from the IRAF `ccdred` package. We then ran the `SExtractor v2.5` code (Bertin & Arnouts 1996) on the reduced images to generate object catalogs, and we matched objects from image to image to determine relative photometric zeropoints, using `SExtractor MAG_AUTO` magnitudes. We also astrometrically aligned the world coordinate system (WCS) of each image to that of the first image, using the IRAF `ccmap` task. The images were then remapped and coadded, specifically median-combined, with account made for the relative flux scalings between the images, using the `swarp v2.16` package[2] The final photometric zeropoint was derived by matching objects detected by `SExtractor` in the coadded V-band image with those in the calibrated g- and r-band images from the APO 3.5m telescope; the APO images were themselves calibrated using SDSS matches, as described below in §4.3. Note this bootstrapping method gives a more robust photometric zeropoint as it provides more objects compared to directly matching the Subaru and SDSS data, due to the small size of the Subaru image and the shallow depth of the SDSS data. The g-band `SExtractor` $3''$ aperture magnitudes were first transformed to V-band, via the relation $V = g - 0.59(g - r) - 0.01$ (Jester et al. 2005), and then used

[2]http://terapix.iap.fr/rubrique.php?id_rubrique=49

to determine the zeropoint of the Subaru image using the V-band magnitude offsets for matching stars and galaxies in the images. The coadded V-band image was astrometrically registered through matches to SDSS objects, again using the IRAF `ccmap` task.

Fig. 3 shows the coadded FOCAS image. Not only is the counter-image A4 now very clear but we can now see that the central lensing galaxy (B) is clearly accompanied by two smaller galaxies (C and D). Our photometry analysis of this image is described below in §4.1.

After the imaging data were obtained, a single 600-sec long-slit FOCAS spectrum was also taken, with the slit oriented to cover both knots A2 and A3 in the arc. The 300B grating and L600 filter were used, providing a dispersion of 1.34Å per pixel, spectral coverage of 3700–6000Å, and a resolution $R \sim 400$ with a $1.0''$-wide slit. The Hubble Space Telescope (HST) spectrophotometric standard G191-B2B was also observed and used for flux calibration. The FOCAS spectroscopic data were reduced using standard routines from the IRAF `twodspec` package. The extracted 1D spectra for the A2 and A3 knots are shown in Fig. 5. The redshift of the arc was found to be $z = 2.0010 \pm 0.0009$ based on measurements of prominent absorption lines due to C II, Si IV, Si II, C IV, Fe II, and Al II, typical features seen in the spectra of star-forming Lyman break galaxies (Shapley et al. 2003), in particular of the $z \sim 2$ "BX/BM" variety as defined by the classification scheme of Steidel et al. (2004). Table 2 summarizes details about the observed lines. The high redshift of the knots, combined with the clear arc morphology seen in the Subaru image, confirm that this is indeed a gravitationally lensed system.

3.2. APO Imaging and Spectroscopy

Additional follow-up imaging data in the SDSS *griz* bands were obtained on the Apache Point Observatory (APO) 3.5m telescope using the SPIcam CCD imager, which has a scale of $0.28''$ per pixel and a field of view of $4.8' \times 4.8'$. The data were obtained under photometric conditions, and the seeing ranged from $0.9''$–$1.2''$. The total exposure time in each filter was 900 sec, divided into three dithered exposures (with $15''$ offsets) of 300 sec each in order to reject cosmic rays and bad pixels. Additional details are given in the observation log in Table 1.

The resulting *griz* images were reduced and coadded using the same procedure described above for the Subaru data. The SPIcam z-band data showed signficant fringing and therefore an additional reduction step was necessary to subtract off a master fringe frame. The final coadded images were again astrometrically registered by matching to SDSS objects.

The photometric zeropoints for the coadded images were derived using unsaturated bright stars in the SPIcam images. Specifically, we used GALFIT (Peng et al. 2002, also see below) to fit Moffat profiles to these stars, and compared the resulting total magnitudes to the corresponding SDSS model magnitudes. Note that we did not apply any color terms in our calibration of SPIcam to SDSS *griz* magnitudes, as verified by a comparison of `SExtractor` photometry of the SPIcam data vs. the corresponding SDSS photometry for matching objects. Fig. 4 shows a montage of the coadded *griz* SPIcam images, as well as a *gri* color composite. We describe our photometry analysis for these images in §4.3 below.

Additional follow-up long-slit spectroscopy of the arc was carried out with the Dual Imaging Spectrograph (DIS III) on the APO 3.5m telescope. Two 600-sec exposures were obtained, with a 1.5″-wide slit covering knots A1 and A2, under ∼1.5″ seeing. The B400/R300 gratings were used, covering an effective spectral range of 3600–9600Å, with a dispersion of 1.83Å per pixel in the blue part of the spectrum and 2.31Å per pixel in the red. The spatial scale is about 0.4″ per pixel. HeNeAr lamp exposures were taken for wavelength calibration, and the spectrophotometric standard stars GD 50 and Feige 110 were observed for flux calibration. The spectra were reduced using the IRAF `ccdred` package and the `doslit` task. The two spectroscopic exposures of the arc were combined using the `scombine` task, and the red and blue spectra were spliced together using the `spliceSpec` task from Gordon Richard's `distools` external IRAF package. The reduced spectrum is shown in Fig 5. As with the Subaru spectra, a redshift was determined from the combined APO spectrum using absorption features typical of Lyman break galaxies (see Table 2). The APO spectrum yields a redshift of $z = 2.0001 \pm 0.0006$, consistent with that from the Subaru spectra.

4. Modeling the System

4.1. Subaru Photometry

We proceed next to derive a lensing model for the Clone system and to measure the photometric properties of the lensing galaxies and the lensed images. The first step is to model the lens components of the image so that their light can be subtracted off, leaving us with just the light of the lensed images that we can use to derive the lensing model, as described below in §4.2. To model the lensing galaxies we have used the GALFIT program (Peng et al. 2002). GALFIT can perform a simultaneous fit to multiple objects in a FITS image. It allows the user to fit a number of common galaxy profiles such as Sersic, de Vaucouleurs, and exponential disk. The inputs required are a FITS image of the system, a FITS file of the point spread function (PSF), an optional mask which can be used to eliminate pixels from consideration in the fit, and a determination of the sky background.

The initial object positions were determined using SExtractor. The modeling was done using the coadded V-band Subaru image as it has the highest resolution. The PSF was determined from stars in the image. We also included the arc and counter-image in the GALFIT model, but did not include the two faint galaxies that can be seen in the bottom right of Fig 3. The best description of the system is obtained using a Sersic profile for the main LRG, de Vaucouleurs profiles for the two small galaxies (C and D), and a combination of 5 exponential disks for the arc and one exponential disk for the counter-image. This gives a χ^2/dof of 1.13. In Table 3 we show the fitted parameters and in Fig. 6 we show the model and the data–model residual image. From the residual image we can see that the galaxies B, C, and D are well modeled, but that the exponential disk model for the arcs is not perfect. We then subtract off the models for just the lens objects B, C, and D from the image, leaving us with the light of the lensed arc and counter-image for the subsequent lens modeling.

4.2. Lens Modeling

We have modeled the lens using the LENSVIEW program (Wayth & Webster 2006), a program for modeling resolved gravitational lenses. It is based on the LENSMEM algorithm (Wallington et al. 1996) and uses a maximum entropy constraint to find the best fitting lens mass model and source brightness distribution. It supports a number of common mass models. The inputs to the program are a FITS image of the lensing system with the non-arc objects removed (Fig. 7, left plot), a FITS file containing the PSF for the image, a FITS image of the pixel-by-pixel variance of the data, an empty FITS image with the dimensions of the desired source plane, and a FITS image containing a mask of the pixels over which the χ^2 will be calculated (Fig. 7, right plot). It also requires the ratio of the angular size of the pixels between the image and source planes. We have used a source plane of 10×10 pixels, with $0.052''$ per pixel, i.e., 4 times finer than the image plane pixel scale.

Using LENSVIEW we have modeled the system using a singular isothermal ellipsoid (SIE; Kormann et al. 1994) as the mass model. The best fit model yields an Einstein radius of $\theta_{\rm Ein} = 3.82 \pm 0.03''$, which translates to $R_{\rm Ein} = 14.8 \pm 0.1\ h^{-1}$ kpc at the LRG redshift of 0.422. The fitted axis ratio and position angle are 0.751 ± 0.018 and $-70.11 \pm 0.39^\circ$ (E of N), respectively. The best fit model with the tangential critical curve is shown in Fig. 8, left plot, and the predicted source with the corresponding tangential caustic is given in Fig. 8, right plot. The best-fit lens center is offset by a small amount, $(0.07'', 0.04'')$ in (RA,Dec), which is much less than 1 pixel (recall the scale is $0.208''$ per pixel) from the center of the LRG light distribution obtained from GALFIT. The total magnification of the system, obtained by dividing the total flux in the arcs by the total flux in the source, is 27 ± 1.

Comparing Fig. 7 (left) and Fig. 8 (left), we see that the model does look qualitatively quite like the data. The best fit χ^2/dof is 2.18 (2102 for 968 dof), however, indicating formally a poor fit. This can be understood by looking at the pixel-by-pixel residuals scaled by the errors, $(\text{counts}_{data} - \text{counts}_{model})/\sigma_{data}$, shown in Fig. 9. We see that there are large residuals coming from the A3 knot, which is brighter in the data than in the model by 23% within a $3''$ aperture. We have explored other mass models including SIE+external shear but find similar or worse agreement.

In strong lensing it has been known for some years that the smooth mass models fit the image positions well but not always the flux ratios of the images. As LENSVIEW uses the full image information it is not possible to use it to determine how well the image positions alone are determined. So we turn to gravlens/lensmodel (Keeton et al. 2001) which allows us to fit an SIE model using only the image positions. We use the A1-A4 image positions determined by running `SExtractor` on the Subaru image and given in Table 4 (same as used below in §4.3). We assign large errors to the flux ratios so that they do not contribute to the χ^2. We obtain a very good fit to the image positions, with a χ^2 of 2.55 for 3 dof and values of the SIE parameters that agree with those from the LENSVIEW fit. As the image positions are well determined, the statistical errors quoted above for our lens model parameters are from the lensmodel fit rather than the LENSVIEW fit. The predicted flux for A3 in the lensmodel fit is smaller than the measured flux by a factor of 2. This is more discrepant than what we obtained from LENSVIEW above, in which the source light distribution is more realistically modeled as an extended source, as opposed to a point source as used in lensmodel. The A3 flux is also not better matched by adding external shear or by adding galaxies C and D as singular isothermal spheres. An interesting discussion of anomalous flux ratios in 4-image lenses with a fold configuration, as is the case for our system, can be found in Keeton et al. (2005). They define the ratio $R_{fold} = (F_+ - F_-)/(F_+ + F_-)$, where F_+ and F_- are the observed fluxes for a pair of images of opposite parity, as indicated by the subscripts. They model R_{fold} for different image pairs in 4-image lenses. Deviations from the expected values are thought to indicate the presence of structure at scales smaller than the separation between the images. We measure $R_{fold} = 0.173$ for the image pair A3-A2. This value is not consistent with the range of values shown in Fig. 5 of Keeton et al. (2005). Given this result and our poor χ^2 from LENSVIEW we conclude that we may have substructure in the lens which is currently not being well modeled using a smooth SIE mass distribution.

From the SIE model, the velocity dispersion of the mass distribution doing the lensing is 440 ± 7 kms^{-1}, which would be quite large for an elliptical galaxy. The SDSS database does not provide a spectroscopic velocity dispersion for the LRG due to the low signal-to-noise of the SDSS spectrum. We obtained a similarly large value for the velocity dispersion of the 8 o'clock arc lensing mass, which is discussed in Allam et al. (2007). Combined with the

large 3.82″ Einstein radius and the presence of neighboring red galaxies like C, D, E (see §4.3), and others further away, this indicates that the lensing is due in part to the group environment around the central LRG (see, e.g., Oguri 2006). We have thus investigated two alternative mass models to attempt a better approximation of the group lensing contribution, specifically using SIE+external shear and a Navarro, Frenk, & White (NFW) profile (Navarro et al. 1997). However, the LENSVIEW fits in both cases give about 10% worse χ^2 per dof than the simple SIE model, and in particular the SIE+external shear model gives only a small shear of 0.006 that is closely aligned with the position angle of the main SIE profile. We will further investigate the group lensing environment, as well as the substructure issues noted above, using higher-resolution HST imaging data that we are analyzing for this system (Allam et al. 2008). Nonetheless, using the current data and a simple SIE fit, we are able to provide a reasonable model that reproduces the most salient features of the lensing system, namely the positions and morphology of the lensed arc and counter-image.

Since both the redshift of the LRG and the source are known we are able to determine the angular diameter distance to the source (D_s), to the lens (D_l), and between the source and lens (D_{sl}), to be 1209, 801 and 829 h^{-1} Mpc, respectively. Then from the simple SIE model we can determine the mass interior to $R_{\rm Ein}$ using $M_{\rm Ein} = (c^2/4G)(D_l D_s/D_{sl}) \times \theta^2_{\rm Ein} = 2.10 \pm 0.03 \times 10^{12}\ h^{-1} M_\odot$. As we are using the SIE convention of Kormann et al. (1994), to be more precise the enclosed mass is actually defined within an elliptical aperture with semi-major axis $\theta_{\rm Ein}$, and axis ratio and position angle as given above. For the same aperture, we also determine the lens light, by summing the fluxes from the best-fitting GALFIT models for the LRG and for galaxies C and D (see § 4.1 and 4.3); the results are given in Table 4. Note that due to the similarity of the Einstein radius of the lens mass model to the half-light (or effective) radius of the LRG, and likewise for the respective axis ratios and position angles (cf. Table 3), the flux within the lens light aperture is very close to half the total flux of the LRG (galaxies C and D contribute only a small amount). We then convert the apparent lens light to absolute fluxes, adopting k-corrections using an elliptical galaxy template (Coleman et al. 1980), and obtain mass-to-light ratios in the rest-frame $gVriz$ bands of $M/L = 27, 22, 19, 15$, and 12 $h\ M_\odot/L_\odot$, respectively ($\Omega_M = 0.3, \Omega_\Lambda = 0.7$). We note that these M/L values, out to a radius of 15 h^{-1} kpc, are ∼5-10 times larger than those for the lensing LRGs, on the scale of a few kpc, from the SLACS sample (Treu et al. 2006; Koopmans et al. 2006). As shown Fig. 7.8 of Kubik (2007), this trend of M/L with radius is consistent with that determined for elliptical galaxies using independent dynamical and X-ray techniques (Bahcall et al. 1995).

4.3. APO Photometry

We turn now to the photometry analysis of the APO 3.5m SPIcam coadded imaging data in order to derive color information for the various lensing galaxies and lensed image components. Because the SPIcam data were taken under only modest seeing conditions, we will rely on the galaxy profile parameters determined earlier from running GALFIT on the Subaru V-band image, rather than try to re-fit those parameters independently in each of the SPIcam $griz$ images. Specifically, we adopt all the best-fit V-band profile parameters for the LRG (= galaxy B), galaxies C and D, and counter-image A4, *except* that we will fit for the total magnitude of each of those four components. Moreover, we also re-fit for the position of the LRG, in order to account for small errors in the astrometric registration relative to the Subaru image; we find best-fit shifts of $\leq 0.07''$, which are small but nonetheless result in noticeable visual improvement in the residual image after subtracting off the LRG model. Note we do not attempt to fit models to the lensed arc images, as was done for the Subaru data. Instead, we mask out the image areas corresponding to the A1, A2, and A3 components before running GALFIT on the SPIcam data. The masks are derived using `SExtractor`-generated "segmentation" images, which flag the pixels belonging to each detected object. We will later compute aperture magnitudes for the arc components, in a model-independent way as described below. For the PSF model needed by GALFIT, we use the best-fit Moffat profile derived by GALFIT for a bright unsaturated star in a given image. We find that our results are not sensitive to whether we use the Moffat profile or the actual data for the star itself as the PSF model. Note we also first use `SExtractor` to do sky subtraction on an image before feeding it to GALFIT. Our GALFIT photometry results for the SPIcam coadded $griz$ images are given in Table 4. We plot the $gVriz$ total magnitudes of the LRG and of galaxies C and D in Fig. 10, where we have also overlaid a template elliptical galaxy spectrum from Coleman et al. (1980), after redshifting to the LRG redshift $z = 0.422$ and converting the flux of the spectrum to AB magnitude units. The reasonable match of the spectral energy distributions (SEDs; described by the $gVriz$ magnitudes) of galaxies C and D to the template spectrum is consistent with the interpretation of those two galaxies as early-type galaxies at the same redshift as the LRG.

As noted above, for the lensed arc image components A1-A3, we measure simple aperture magnitudes. We do this instead of attempting profile fitting since we do not expect the lensed and distorted arc images to follow standard galaxy profiles, as can be seen in the residual image shown in Figure 6 (right panel) for the Subaru data. We measure $3''$-diameter circular aperture magnitudes for each of the A1-A3 arc components, with centers determined from running `SExtractor` on the Subaru image. The aperture magnitudes are measured from the images after subtraction of the best-fit GALFIT galaxy models as described above. The Subaru V-band image is first convolved by a Gaussian to degrade the seeing to $1.0''$ to

match the typical seeing in the SPIcam data. Otherwise no aperture corrections are made to reconcile the small seeing differences among the $griz$ data. We also ignore a small overlap in the apertures centered on the A1 and A2 components and do not attempt any deblending. In addition, we define a partial annular aperture, centered on the LRG, with inner radius $3''$, outer radius $5.5''$, and position angle ranging from -140 to $+5$ degrees E of N. This (partial) annulus provides a simple aperture that captures the shape and flux of the lensed arc. Our aperture photometry results for lensed arc images are presented in Table 4.

We see from Fig. 11 that the lensed A3 component and the counter-image A4 show excellent agreement in their SEDs, as described by their $gVriz$ magnitudes. This also gives us confidence that our GALFIT galaxy fitting and model subtraction procedure is working well, as A4 is significantly fainter than A3 and one might have expected that A4's photometry is prone to proportionately more error due to contamination by the light of the LRG. However, Fig. 11 also shows that the A2 and especially the A1 components are significantly redder than the A3 component. This may also be seen from Fig. 4, where the upper part of the A1 knot appears noticeably redder than the rest of the arc. It turns out from our higher-resolution HST data (Allam et al. 2008) that there is also a small red galaxy, henceforth galaxy E, inside A1's $3''$ aperture. There is also some flux from galaxy E contaminating the A2 aperture due to seeing. Although galaxy E is not resolved from the arc even in our best-seeing ground-based data, the Subaru image, we can nonetheless infer its brightness by assuming it has the same SED as the LRG. We therefore decompose the flux within the A1, A2, and annular apertures as a linear combination of two flux components: one with the SED of A3 to account for the lensed source galaxy flux, and the other with the SED of the LRG to account for the galaxy E flux. Doing this allows us to "decontaminate" the galaxy E flux from the A1, A2, and annular apertures. As shown in Fig. 11, this procedure produces good fits to the total fluxes within the A1, A2, and annular apertures, and in that figure and in Table 4 we also show the "decontaminated" fluxes obtained by subtracting the best-fit LRG-component flux from the original fluxes within each of those apertures. Note that this is not a trivial result as the procedure uses only two parameters (the two flux components) to fit the five data points (the $gVriz$ fluxes) for each aperture. Also, from the annulus result we find that the galaxy E flux is about 2% of the LRG flux, making galaxy E comparable to galaxies C and D in brightness (see Table 4). In the V-band, the galaxy E flux contaminating the annular aperture is about 6% of the lensed source galaxy flux, implying only a small perturbation for the LENSVIEW modeling results presented above using the Subaru image.

5. Source Galaxy Star Formation Rate

To estimate the star formation rate (SFR) and the amount of dust extinction, we compare our $gVriz$ SED data to models from the GALAXEV (Bruzual & Charlot 2003) stellar population evolution package. We use simple constant star formation rate models, with solar metallicity and a Salpeter (1955) initial mass function (IMF) over the mass range $0.1-100\ M_\odot$, and we also add dust extinction according to the prescription of Calzetti et al. (2000). We consider ages of 10 Myr, 100 Myr, and 1 Gyr for the models, and set values of the (stellar continuum) color excess $E(B-V)$ to 0.3, 0.25, and 0.2, respectively, in order to get a good visual match to the slope of the $gVriz$ data for the annulus aperture; see Fig. 12. We set the normalization of each model by finding the average offset between the observed and model $gVriz$ magnitudes. To facilitate comparison with previous simple SFR estimates for cB58 and the 8 o'clock arc, we express our results in analogy with eqn. (6) of Pettini et al. (2000), but using a flat cosmology with $\Omega_M = 0.3, \Omega_\Lambda = 0.7$, and $H_0 = 100h$ km s^{-1} Mpc^{-1},

$$\mathrm{SFR} \approx 32 \times \left(\frac{24}{f_{\rm lens}}\right) \times \left(\frac{f_{\rm dust}}{11}\right) \times \left(\frac{7.8\times10^{27}\ \mathrm{erg\ s^{-1}\ Hz^{-1}}}{F_{\nu,1500}}\right) \times \left(\frac{2.5}{f_{\rm IMF}}\right) h^{-1}\ M_\odot\ \mathrm{yr}^{-1}\ , \quad (1)$$

where $f_{\rm lens}$ is the lensing magnification corresponding to the flux inside the annulus aperture, $f_{\rm dust}$ is the extinction at rest wavelength 1500 Å, $F_{\nu,1500}$ is the flux at rest 1500 Å for a model forming stars at 1 $M_\odot$ yr^{-1}, and $f_{\rm IMF}$ is a correction factor to the Salpeter IMF, as described by Pettini et al. (2000) and references therein. The numerical values given in eqn. (1) are for our fiducial model with an age of 100 Myr and $E(B-V) = 0.25$. The corresponding numbers for the 10 Myr, $E(B-V) = 0.3$ and 1 Gyr, $E(B-V) = 0.2$ models are, respectively: $\mathrm{SFR} = 18, 83\ h^{-1}\ M_\odot\ \mathrm{yr}^{-1}$; $f_{\rm dust} = 17, 6.7$; and $F_{\nu,1500} = 4.9, 8.6 \times 10^{27}$ erg s^{-1} Hz^{-1}.

As shown in Fig. 12, although an example dust-free 100 Myr model is clearly ruled out, all three of the dusty models considered give good matches to the data and cannot be distinguished given our data, which cover just rest-frame UV wavelengths. We defer a fuller model-fitting analysis to a future paper that will also include the imaging and spectroscopic data we have obtained at observed-frame IR = rest-frame optical wavelengths, which will allow us to set much more stringent constraints on model ages, dust extinction and star formation rates (e.g., Ellingson et al. 1996). Nevertheless, we can still compare star formation rates obtained under similar assumptions for other systems. In particular, for the fiducial 100 Myr model, the resulting SFR of 32 $h^{-1}\ M_\odot$ yr^{-1} is about twice the value of 17 $h^{-1}\ M_\odot$ yr^{-1} obtained by Pettini et al. (2000) for cB58 (after converting to our adopted cosmology), but it is much lower than the 160 $h^{-1}\ M_\odot$ yr^{-1} obtained by Allam et al. (2007) for the 8 o'clock arc. We can also compare our source galaxy with the sample of about 100 (unlensed) $z \sim 2$ star-forming galaxies of Erb et al. (2006a,b), who derived SFRs using detailed SED fitting with Bruzual & Charlot (2003) models, including additional IR data in the fits. The bulk

of the Erb et al. (2006a,b) sample galaxies were best fit with constant SFR models like the ones we have used. Overall those galaxies have a mean best-fit age of 1046 Myr, $E(B-V)$ of 0.15 and SFR of 52 $M_\odot$ yr^{-1} ($H_0 = 70$ km s^{-1} Mpc^{-1}), which becomes 26 $h^{-1}M_\odot$ yr^{-1} after converting to our conventions.[3] We see that our source galaxy appears somewhat dustier, but otherwise it has a star formation rate close to the typical $z \sim 2$ star-forming galaxy from the Erb et al. (2006a,b) sample.

6. Conclusions

We have reported on the discovery of the Clone system, consisting of a star-forming, BX/BM-type Lyman break galaxy in the SDSS at a redshift of $z = 2.001$, which is strongly lensed by a foreground luminous red galaxy at a redshift of $z = 0.422$. The lensed galaxy is remarkably bright, and at $r = 19.9$ it is among the brightest known lensed source galaxies with $z \geq 2$.

A simple SIE lens model for the system yields an Einstein radius of $\theta_{\rm Ein} = 3.82 \pm 0.03''$ (or $R_{\rm Ein} = 14.8 \pm 0.1$ h^{-1} kpc at the lens redshift), a total lensing mass within the Einstein radius of $2.10 \pm 0.03 \times 10^{12}$ $h^{-1}M_\odot$, and a magnification factor for the lensed LBG of 27 ± 1. Combining the lens model with our follow-up $gVriz$ photometry, we have also estimated the (unlensed) star formation rate (SFR) of the source galaxy to be 32 h^{-1} $M_\odot$ yr^{-1}, adopting a fiducial constant-SFR galaxy evolution model with an age of 100 Myr and $E(B-V) = 0.25$. Such a star formation rate is similar to that found for samples of similar, but unlensed, $z \sim 2$ BX/BM galaxies.

We are pursuing a number of further follow-up observations on this system, and we currently have optical and infrared data from HST Cycle 16, Spitzer Cycle 4, and Gemini North programs. The HST images indicate that the system is more complex than can be seen from the ground, and analysis of that higher resolution data will help us investigate the issues of substructure and image flux anomalies that we have encountered in the lens modeling described here. Moreover, we will also use the SED information provided by the additional near-IR imaging and spectroscopy we are analyzing to better constrain the star formation history and dust content than we have been able to do here using just the optical data. These more detailed analyses will be the subjects of future papers that will exploit the rich follow-up data set that can be derived from this very bright high-redshift lensing

[3]We account for H_0, for a factor of 1.8 to convert the SFR normalization from the Chabrier (2003) IMF used by Erb et al. (2006a,b) back to a Salpeter IMF, and finally for our use of the factor $f_{\rm IMF} = 2.5$ from Pettini et al. (2000).

system.

SSA acknowledges support from a HST Grant. Support for program #11167 was provided by NASA through a grant from the Space Telescope Science Institute, which is operated by the Association of Universities for Research in Astronomy, Inc., under NASA contract NAS5-26555.

This work was supported in part by Department of Energy contract DE-AC02-76SF00515.

These results are based on observations obtained with the Apache Point Observatory 3.5-meter telescope, which is owned and operated by the Astrophysical Research Consortium.

Based [in part] on data collected at Subaru Telescope, which is operated by the National Astronomical Observatory of Japan.

Funding for the SDSS and SDSS-II has been provided by the Alfred P. Sloan Foundation, the Participating Institutions, the National Science Foundation, the U.S. Department of Energy, the National Aeronautics and Space Administration, the Japanese Monbukagakusho, the Max Planck Society, and the Higher Education Funding Council for England. The SDSS Web Site is http://www.sdss.org/. The SDSS is managed by the Astrophysical Research Consortium for the Participating Institutions. The Participating Institutions are the American Museum of Natural History, Astrophysical Institute Potsdam, University of Basel, University of Cambridge, Case Western Reserve University, University of Chicago, Drexel University, Fermilab, the Institute for Advanced Study, the Japan Participation Group, Johns Hopkins University, the Joint Institute for Nuclear Astrophysics, the Kavli Institute for Particle Astrophysics and Cosmology, the Korean Scientist Group, the Chinese Academy of Sciences (LAMOST), Los Alamos National Laboratory, the Max-Planck-Institute for Astronomy (MPIA), the Max-Planck-Institute for Astrophysics (MPA), New Mexico State University, Ohio State University, University of Pittsburgh, University of Portsmouth, Princeton University, the United States Naval Observatory, and the University of Washington.

REFERENCES

Adelman-McCarthy, J., et al. 2006, ApJS, 162, 38

Adelman-McCarthy, J., et al. 2007, ApJS, 172, 634

Allam, S., et al. 2007, ApJ, 662, 51

Allam, S., et al. 2008, in preparation

Bahcall, N. A., Lubin, L. M., & Dorman, V. 1995, ApJ, 447, L81

Belokurov, V., et al. 2007, ApJ, 671, L9

Bertin, E., & Arnouts, S. 1996, A&AS, 117, 393

Bolton, A. S., et al. 2006, ApJ, 638, 703

Bruzual, G., & Charlot, S. 2003, MNRAS, 344, 1000

Calzetti, D., Armus, L., Bohlin, R. C., Kinney, A. L., Koornneef, J., & Storchi-Bergmann, T. 2000, ApJ, 533, 682

Chabrier, G. 2003, PASP, 115, 763

Coleman, G. D., Wu, C.-C., & Weedman, D. W. 1980, ApJS, 43, 393

Ellingson, E., Yee, H. K. C., Bechtold, J., & Elston, R. 1996, ApJ, 466, L71

Erb, D. K., Steidel, C. C., Shapley, A. E., Pettini, M., Reddy, N. A., & Adelberger, K. L. 2006a, ApJ, 646, 107

Erb, D. K., Steidel, C. C., Shapley, A. E., Pettini, M., Reddy, N. A., & Adelberger, K. L. 2006b, ApJ, 647, 128

Fukugita, M., Ichikawa, T., Gunn, J. E., Doi, M., Shimasaku, K., & Schneider, D. P. 1996, AJ, 111, 1748

Hansen, S. M., et al. 2005, ApJ, 633, 122

Jester, S., et al. 2005, AJ, 130, 873

Kashikawa, N., et al. 2002, PASJ, 54, 819

Keeton, C. R. 2001, arXiv:astro-ph/0102340

Keeton, C. R., Gaudi B. S., & Petters, A.O. 2005, ApJ, 635, 35

Koester, B. P., et al. 2007, ApJ, 660, 221

Koopmans, L. V. E., et al. 2006, ApJ, 649, 599

Kormann, R., Schneider, P., & Bartelmann, M. 1994, A&A, 284, 285

Kubik, D. 2007, M.S. Thesis, Northern Illinois University

Morton, D. C. 1991, ApJS, 77, 119

Navarro, J. F., Frenk, C. S., & White, S. D. M. 1997, ApJ, 490, 493

Oguri, M. 2006, MNRAS, 367, 1241

Peng, C., et al. 2002, AJ, 124, 266

Pettini, M., Steidel, C. C., Adelberger, K. L., Dickinson, M., & Giavalisco, M. 2000, ApJ, 528, 96

Salpeter, E. E. 1955, ApJ, 121, 161

Schlegel, D. J., Finkbeiner, D. P., & Davis, M. 1998, ApJ, 500, 525

Shapley, A. E., et al. 2003, ApJ, 588, 65

Smail, I., et al. 2007, ApJ, 654, L33

Steidel, C. C., et al. 2003, ApJ, 592, 728

Steidel, C. C., Shapley, A. E., Pettini, M., Adelberger, K. L., Erb, D. K., Reddy, N. A., & Hunt, M. P. 2004, ApJ, 604, 534

Teplitz, H. I., et al. 2000, ApJ, 533, L65

Treu, T., et al. 2006, ApJ, 640, 662

Wallington, S., et al. 1996, ApJ, 465 64

Wayth, R., & Webster, R.L. 2006, MNRAS, 1187, 372

Yee, H. K. C., et al. 1996, AJ, 111, 1783

York, D. G., et al. 2000, AJ, 120, 1579

This preprint was prepared with the AAS LaTeX macros v5.2.

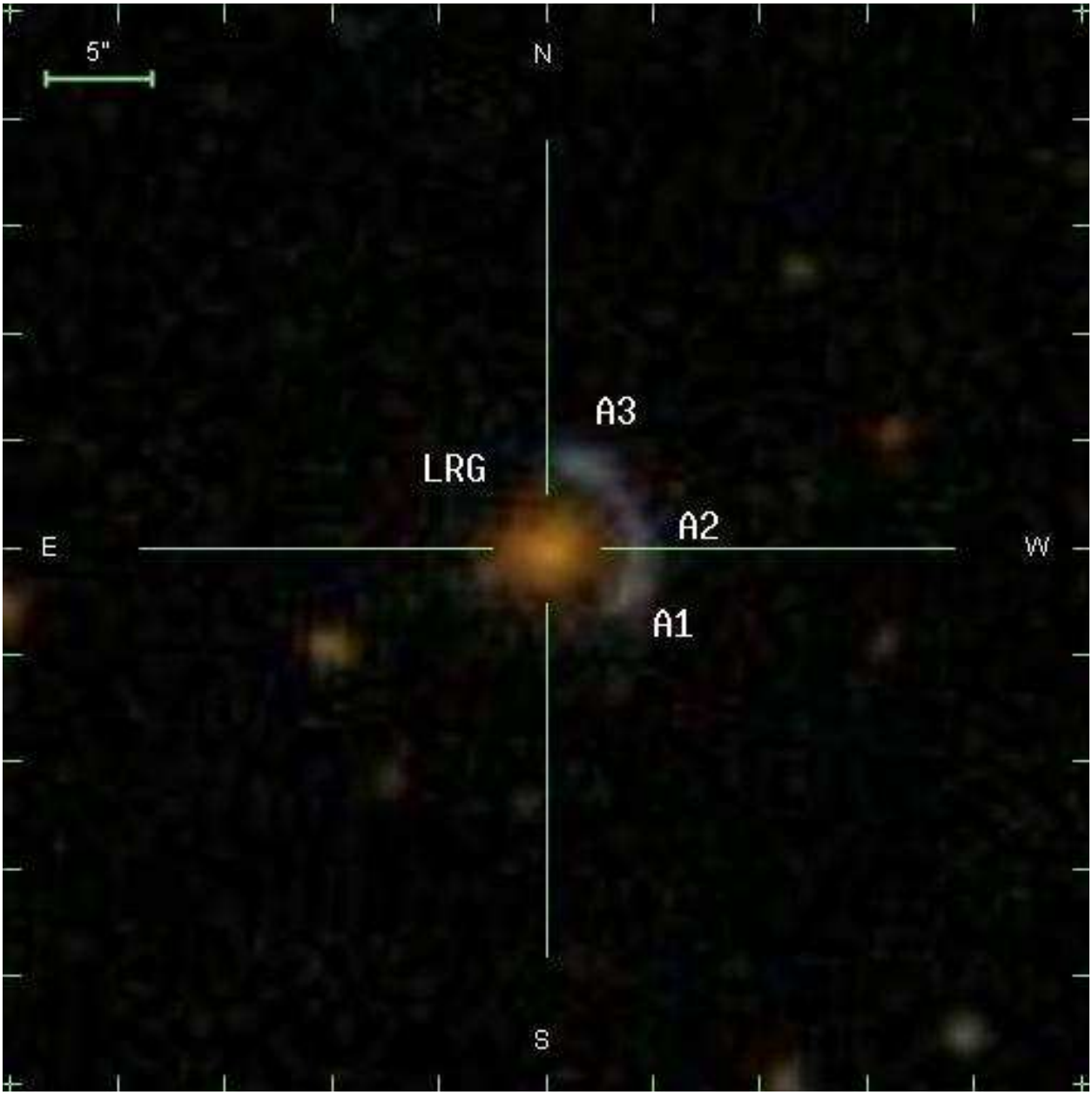

Fig. 1.— The SDSS *gri* color composite image (provided by the SDSS `SkyServer`) from which the arc was discovered. Labels have been added to indicate the locations of the three lensed arc components (A1, A2, and A3) and the position of the LRG.

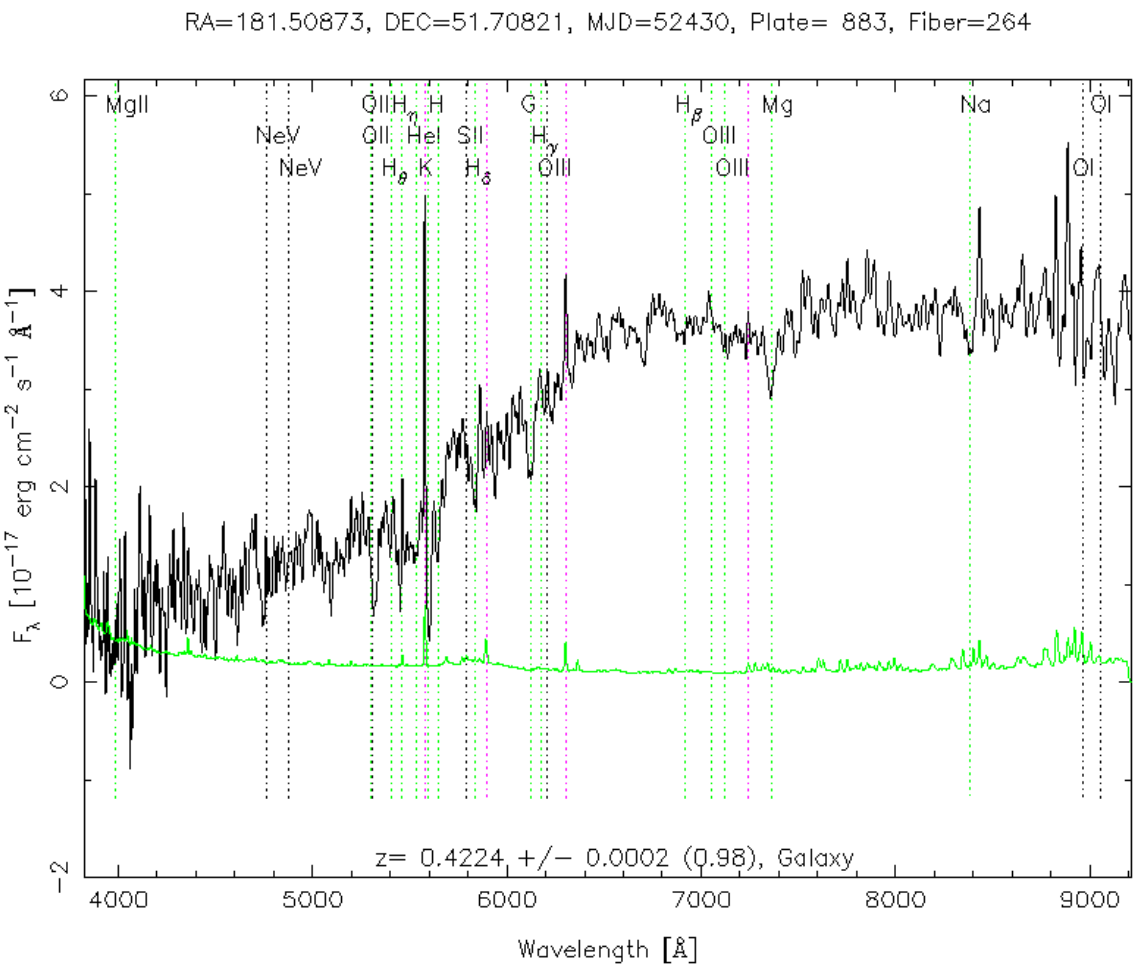

Fig. 2.— The SDSS spectrum (provided by the SDSS `SkyServer`) of the LRG, showing an early-type galaxy spectrum with a redshift $z = 0.4224 \pm 0.0002$. The labels and vertical green lines indicate potential spectral features (whether present or not) at the LRG redshift. Note that the prominent emission feature at ∼5577Å is really a strong night sky line subtraction residual, as indicated by the vertical magenta lines.

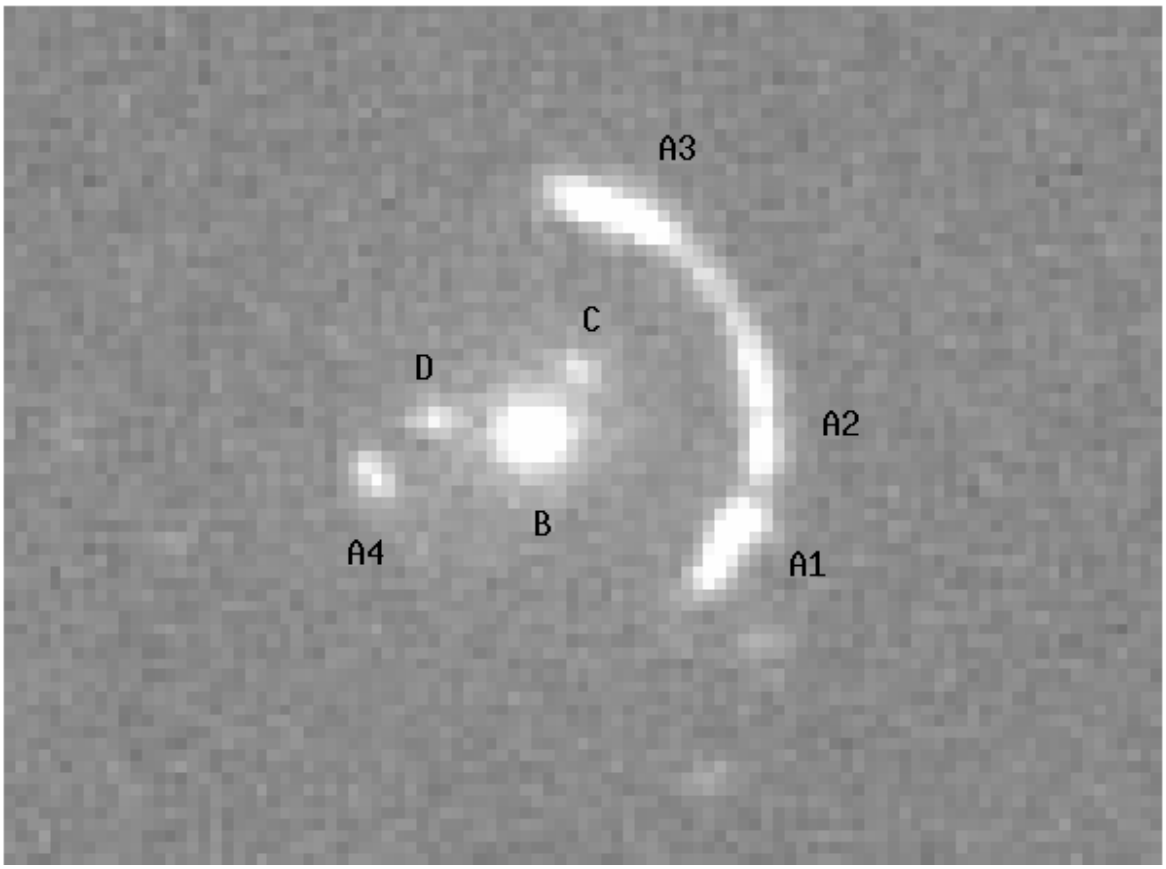

Fig. 3.— The coadded FOCAS V-band image. The arc components are labelled A1, A2, and A3, and the counter-image is A4. The three central galaxies are labelled B (LRG), C, and D.

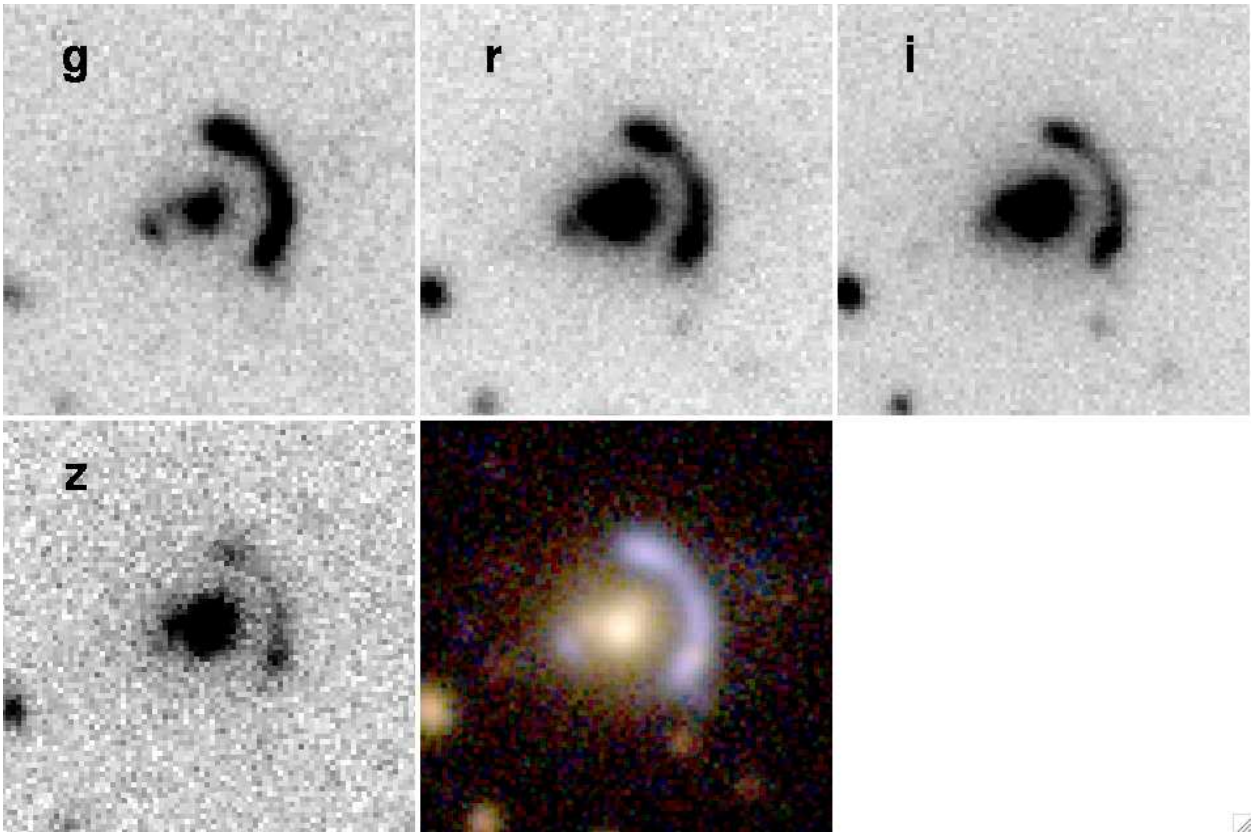

Fig. 4.— The coadded SPIcam *griz* images and *gri* color composite. Note the prominent blue color of the lensed arc and counter-image contrasted with the redder color of the LRG.

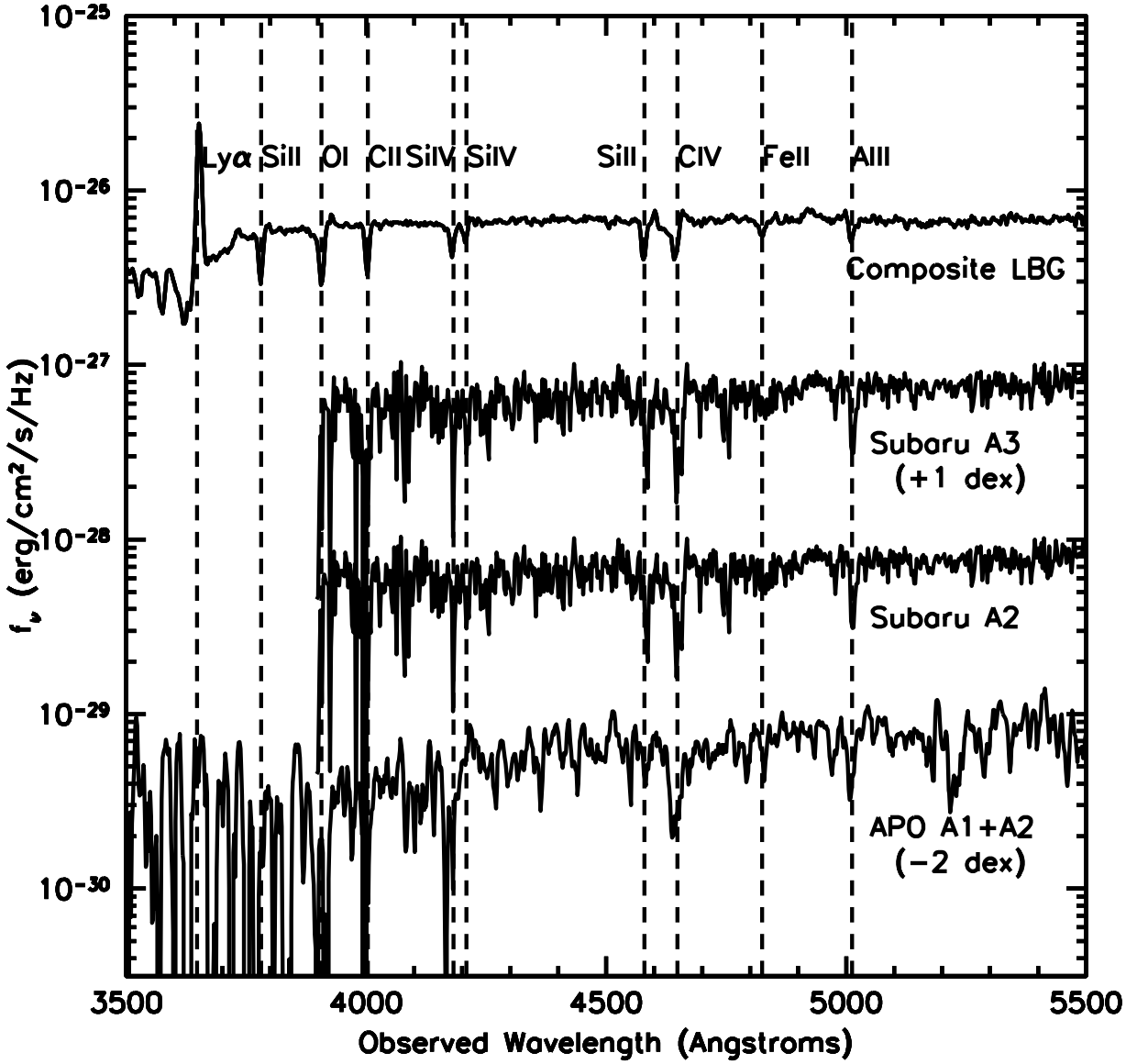

Fig. 5.— Flux-calibrated spectra (in f_ν) for the arc: the Subaru spectra show knots A2 and A3 separately, while the APO 3.5m spectrum combines knots A1 and A2 and has also been smoothed (with a boxcar of 5 pixels = 9Å) to improve S/N. The spectra have been shifted as indicated in the figure labels to improve visibility. A composite LBG spectrum (Shapley et al. 2003), redshifted to $z = 2.00$ to match the arc, is also shown for reference. The prominent spectroscopic features typical of LBGs are labeled and indicated by the vertical dashed lines.

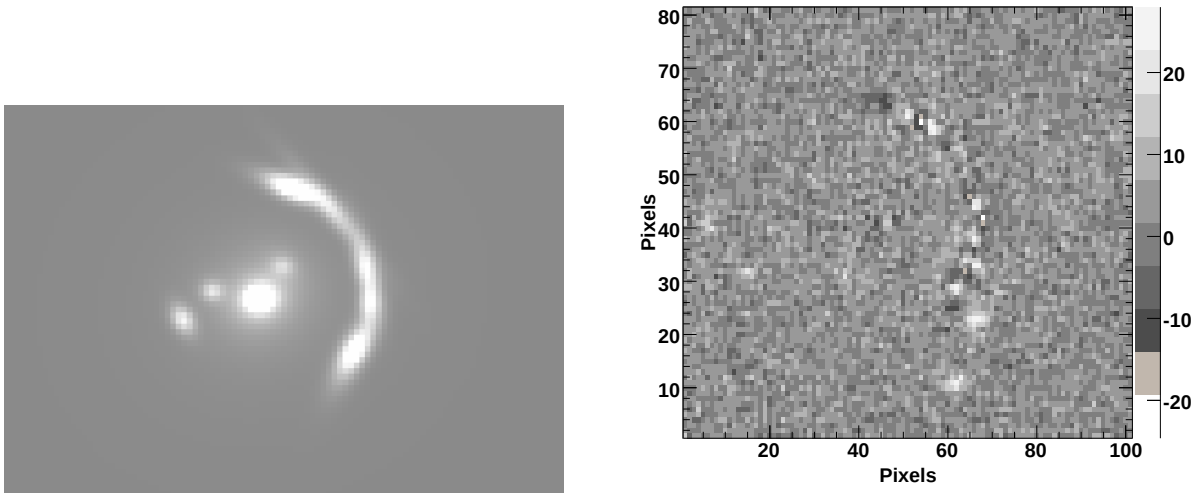

Fig. 6.— The best fit model image (*left*) obtained by running GALFIT on the Subaru V-band image of the system and the resulting data-model residual image (*right*). The scale in the right panel is in units of observed counts per pixel per 15-second exposure time. See §4.1 for details.

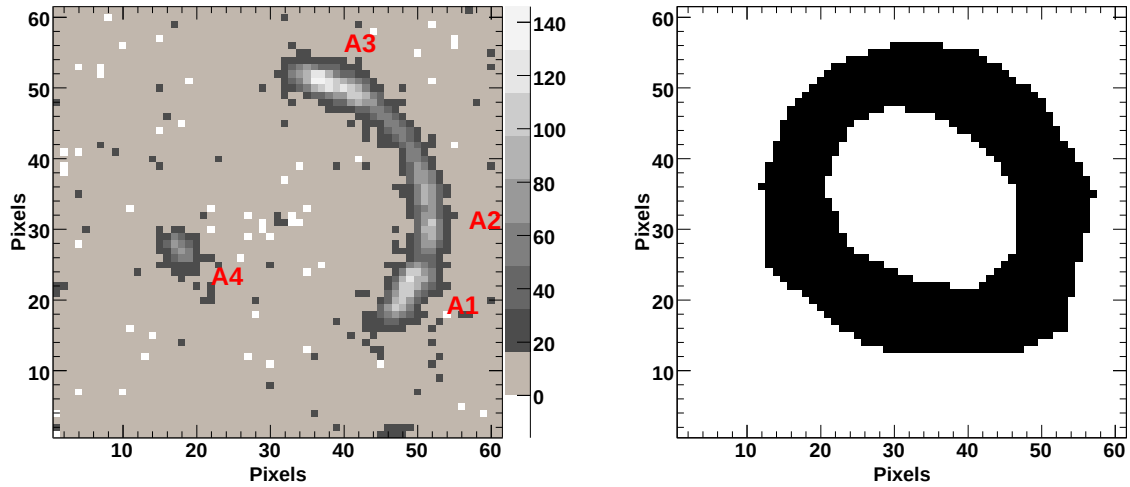

Fig. 7.— The input image (*left*) and the pixel mask (*right*) used in the LENSVIEW lens model fits. LENSVIEW will use only the pixels inside the mask (the black region in the right panel) to calculate the χ^2 between the input image and the model. The scale in the left panel is in units of observed counts per pixel per 15-second exposure for the Subaru V-band image. See §4.2 for details.

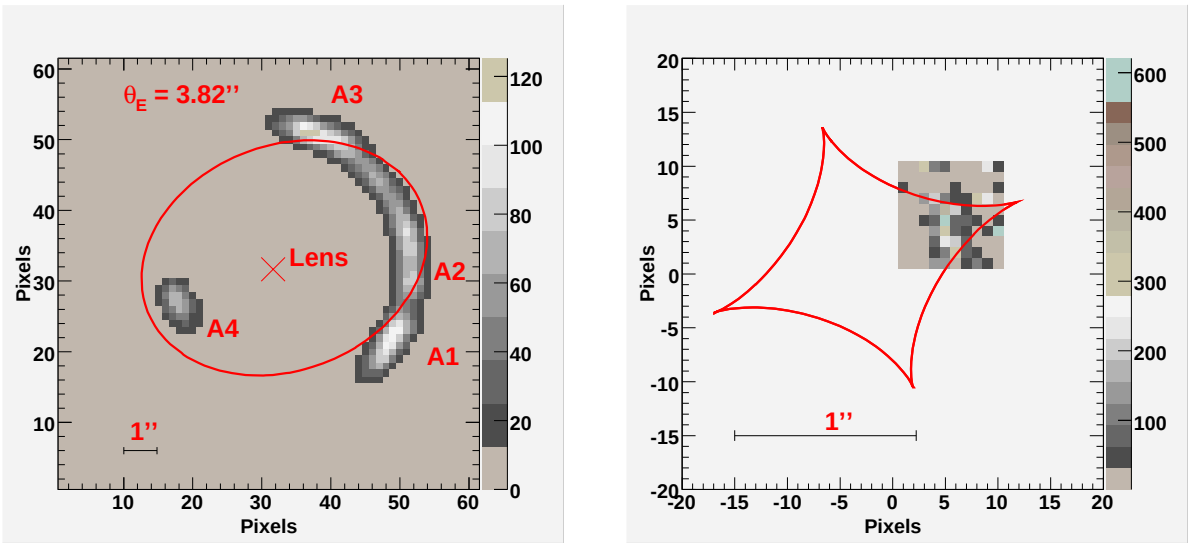

Fig. 8.— The best fit LENSVIEW model image (*left*). The tangential critical line is shown in red. The best fit LENSVIEW model source (*right*). The tangential caustic is shown in red along with the 10×10 pixel source plane. On both plots the spatial scale is indicated by the horizontal bar representing $1''$. The flux scales in the panels are in units of observed counts per *image plane* pixel ($0.208''$ pixel^{-1}) per 15-second exposure for the Subaru V-band image. Note the source plane pixels ($0.052''$ pixel^{-1}) in the right panel are 16 times smaller in area than the image plane pixels in the left panel.

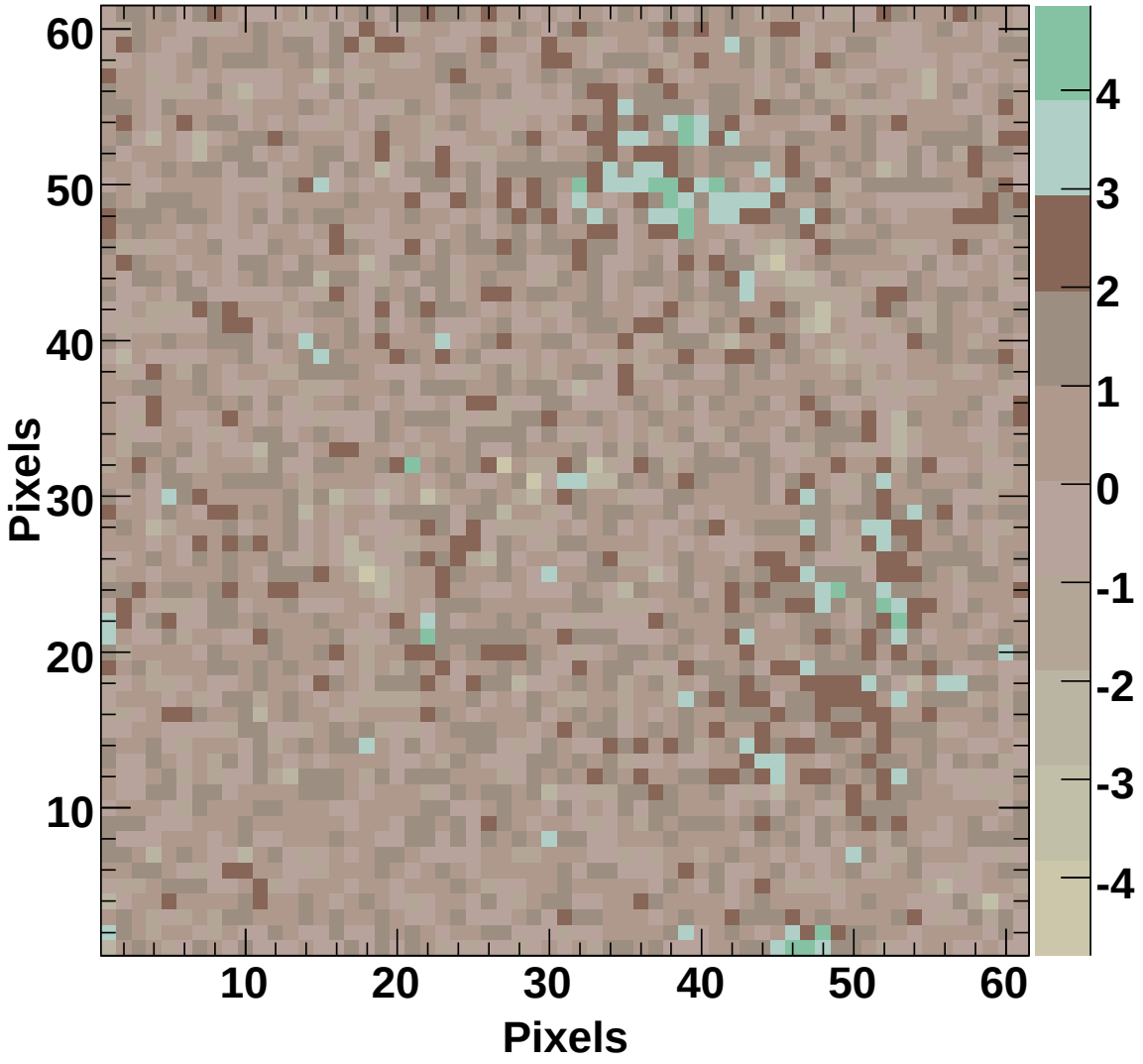

Fig. 9.— The normalized residual image, $(\text{counts}_{data} - \text{counts}_{model})/\sigma_{data}$, for the best fit LENSVIEW model of the system.

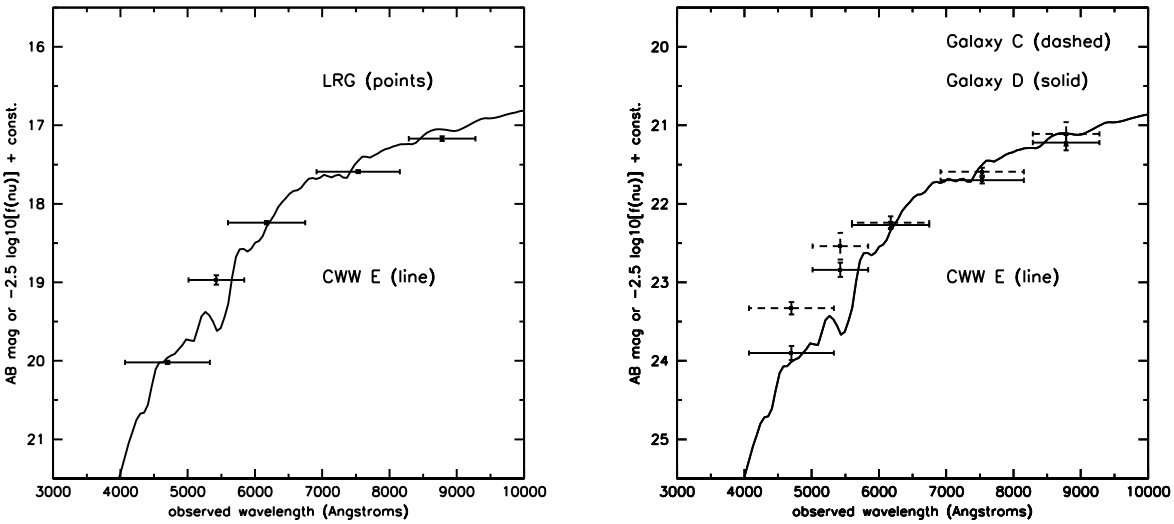

Fig. 10.— The $gVriz$ AB magnitudes (*points with error bars*) of the LRG (*left*) and galaxies C and D (*right*) are compared to the rescaled spectrum of a template elliptical galaxy (CWW E) from Coleman et al. (1980). The CWW E template spectrum has been redshifted to the LRG redshift $z = 0.422$.

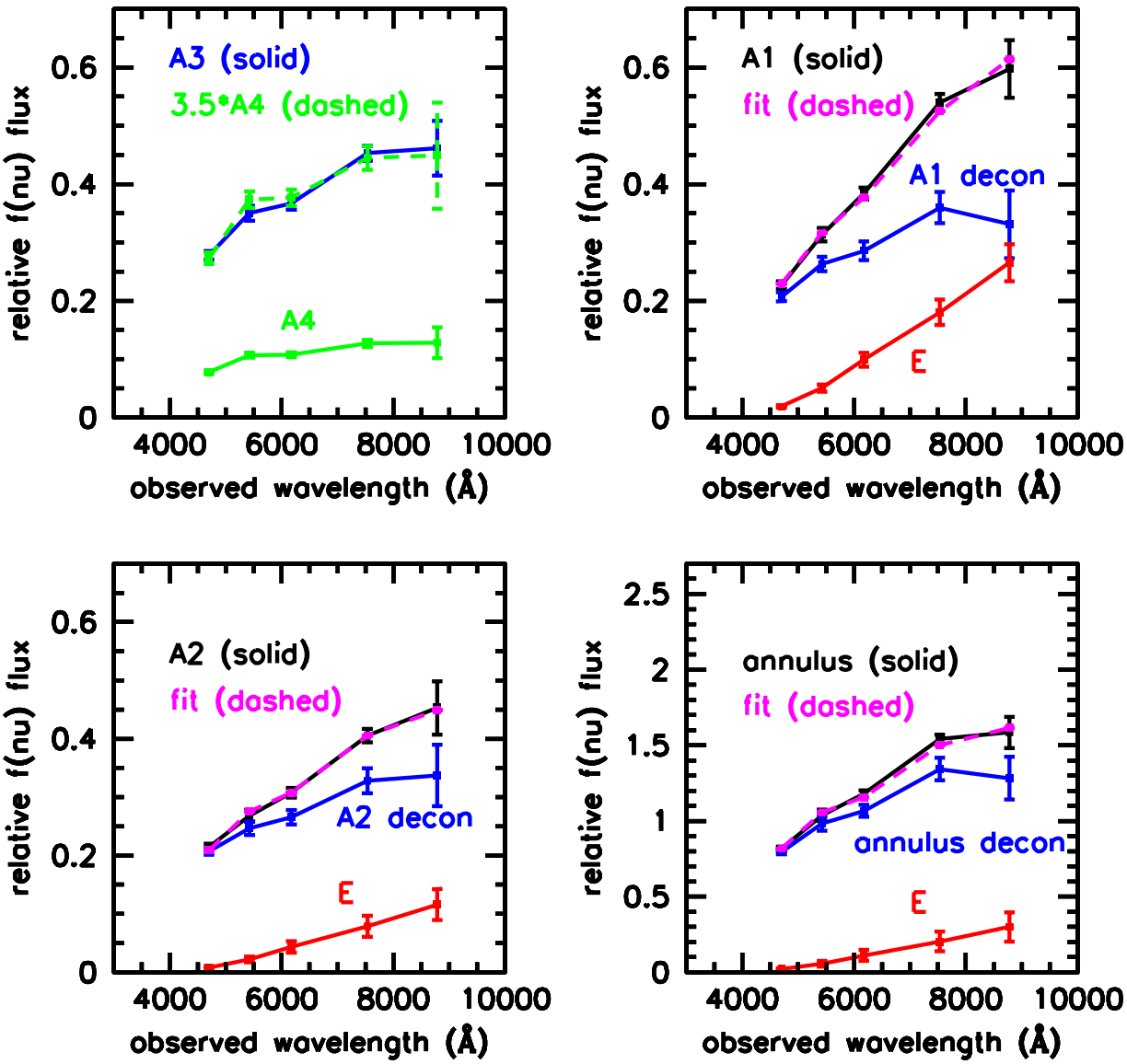

Fig. 11.— The $gVriz$ magnitudes for the lensed image components A1-A4, for a partial annular aperture ("annulus") containing the lensed arc, and for galaxy E are shown. Results are also shown after a fitting procedure is used to decontaminate ("decon") the light of galaxy E from the A1, A2, and partial annulus apertures. Please see §4.3 for the full details. Note the vertical scale is in arbitrary, relative units that are *linear* in the f_ν flux.

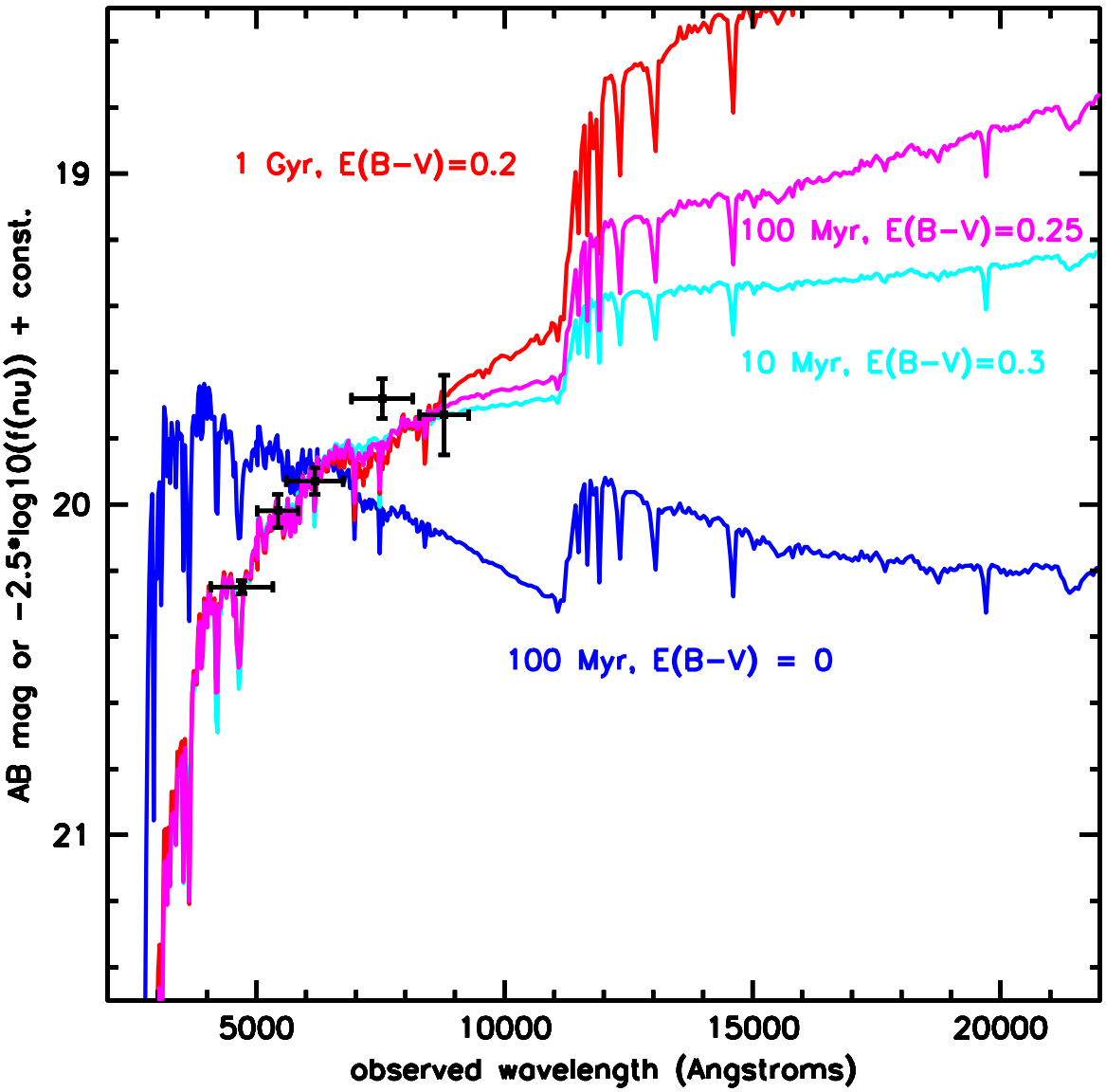

Fig. 12.— The $gVriz$ magnitudes (*black points with error bars*) of the arc in the partial annulus aperture are compared to four different Bruzual & Charlot (2003) constant star formation rate models normalized to the data. The models span a range of different ages and dust extinction values: 100 Myr, $E(B-V) = 0$ (*blue*); 10 Myr, $E(B-V) = 0.3$ (*cyan*); 100 Myr, $E(B-V) = 0.25$ (*magenta*); and 1 Gyr, $E(B-V) = 0.2$ (*red*). See §5 for details.

Table 1. Observation Log

Filter/Grating	UT Date	Exposure	Seeing	Notes
Subaru 8.2m/FOCAS imaging				
V	23 Jan 2007	3×15 sec	0.53″	
Subaru 8.2m/FOCAS spectroscopy				
300B+L600	23 Jan 2007	1×600 sec	0.5″	slit includes knots A2, A3
APO 3.5m/SPIcam imaging				
g	11 Jan 2008	3×300 sec	1.0″	
r	11 Jan 2008	3×300 sec	1.2″	
i	11 Jan 2008	3×300 sec	0.9″	
z	28 Oct 2007	3×300 sec	1.1″	
APO 3.5m/DIS spectroscopy				
B400/R300	19 Nov 2007	2×600 sec	∼1.5″	slit includes knots A1, A2

Table 2. Arc Spectroscopic Features

ID/Rest Wavelength [Å]	Subaru 8.2m (A2+A3) Observed Wavelength[a] [Å]	Redshift	APO 3.5m (A1+A2) Observed Wavelength[a] [Å]	Redshift
Lyα 1215.7	···	···	3650.0[b]	2.0025
SiII 1260.4	···	···	3781.4	2.0002
OI 1302.2, SiII 1304.4	···	···	3904.6	1.9959
CII 1334.5	3999.1	1.9967	4002.6	1.9993
SiIV 1393.8	4180.3	1.9992	4181.8	2.0003
SiIV 1402.8	4210.4	2.0014	4209.1	2.0005
SiII 1526.7	4584.0	2.0026	4581.9	2.0012
CIV 1548.2,1550.8	4650.2	2.0011	4644.7	1.9975
FeII 1608.4	4831.7	2.0040	4827.4	2.0014
AlII 1670.8	5015.6	2.0019	5015.2	2.0017
mean redshift		2.0010±0.0009		2.0001±0.0006

[a] The observed wavelengths were converted from wavelengths in air to wavelengths in vacuum using eq. [3] of Morton (1991).

[b] Lyα is seen in absorption in the APO 3.5m spectrum, with an observed equivalent width of -15 ± 1 Å, or -5 ± 0.3 Å in the rest frame.

Table 3. GALFIT Modeling Results

Object	Model	V Magnitude[a]	Effective Radius r_e (arcsec)	Exponent	Axis Ratio	Position Angle (deg E of N)
B(LRG)	Sersic	18.97 ± 0.05	3.67 ± 0.34	4.68 ± 0.22	0.89 ± 0.01	-68.2 ± 6.2
C	de Vaucouleurs	22.54 ± 0.17	0.56 ± 0.16	4	0.59 ± 0.15	47.3 ± 12.5
D	de Vaucouleurs	22.84 ± 0.09	0.19 ± 0.1	4	0.77 ± 0.2	42.7 ± 34.6
			Scalelength r_s (arcsec)			
Arc (A3)	Exponential	20.88 ± 0.01	0.52 ± 0.01		0.24 ± 0.01	68.4 ± 0.5
Arc	Exponential	21.72 ± 0.04	0.79 ± 0.04		0.05 ± 0.01	39.4 ± 0.66
Arc (A2)	Exponential	21.64 ± 0.07	0.47 ± 0.02		0.15 ± 0.02	12.6 ± 1.2
Arc (A2)	Exponential	21.82 ± 0.08	0.48 ± 0.03		0.03 ± 0.0	6.5 ± 0.6
Arc (A1)	Exponential	20.91 ± 0.01	0.57 ± 0.01		0.22 ± 0.01	-28.0 ± 0.4
Counter-image (A4)	Exponential	22.43 ± 0.03	0.23 ± 0.01		0.28 ± 0.06	25.8 ± 3.2

[a]The photometry errors given here are the formal errors reported by GALFIT. The magnitudes have been corrected for Milky Way extinction, using values from the SDSS DR5 database, which are in turn based on the dust maps of Schlegel et al. (1998). Specifically, the extinction correction in V is 0.070 mag and $E(B-V) = 0.023$.

Table 4. Photometry Results[b,c]

Object[a]	RA (deg)	Dec (deg)	g	V	r	i	z
B (LRG, GALFIT)	181.508732	51.708196	20.02 ± 0.02	18.97 ± 0.06	18.24 ± 0.02	17.59 ± 0.02	17.17 ± 0.03
lens light aperture			20.66 ± 0.03	19.62 ± 0.04	18.92 ± 0.02	18.27 ± 0.02	17.85 ± 0.04
C (GALFIT)	181.508354	51.708526	23.33 ± 0.08	22.54 ± 0.17	22.24 ± 0.08	21.59 ± 0.05	21.11 ± 0.15
D (GALFIT)	181.509529	51.708270	23.90 ± 0.09	22.84 ± 0.09	22.27 ± 0.04	21.70 ± 0.04	21.22 ± 0.10
E (fit)			24.29 ± 0.13	23.24 ± 0.13	22.51 ± 0.13	21.86 ± 0.13	21.44 ± 0.13
A1 ($3''$)	181.507131	51.707665	21.61 ± 0.03	21.26 ± 0.04	21.04 ± 0.03	20.67 ± 0.03	20.56 ± 0.09
A1 (decon, $3''$)			21.71 ± 0.04	21.45 ± 0.05	21.36 ± 0.06	21.11 ± 0.08	21.20 ± 0.19
A2 ($3''$)	181.506902	51.708333	21.67 ± 0.03	21.43 ± 0.04	21.28 ± 0.03	20.98 ± 0.03	20.86 ± 0.11
A2 (decon, $3''$)			21.71 ± 0.03	21.52 ± 0.05	21.44 ± 0.05	21.21 ± 0.07	21.18 ± 0.17
A3 ($3''$)	181.508016	51.709280	21.39 ± 0.03	21.14 ± 0.04	21.09 ± 0.03	20.86 ± 0.03	20.84 ± 0.11
annulus			20.22 ± 0.02	19.96 ± 0.04	19.82 ± 0.02	19.53 ± 0.02	19.50 ± 0.07
annulus (decon)			20.25 ± 0.02	20.02 ± 0.05	19.93 ± 0.04	19.68 ± 0.06	19.73 ± 0.12
A4 (GALFIT)	181.510019	51.707975	22.77 ± 0.04	22.43 ± 0.04	22.42 ± 0.04	22.24 ± 0.05	22.23 ± 0.22

[a]The type of photometry measurement and/or the photometry aperture is indicated in the parentheses next to the object name. Detailed descriptions of the photometry measurements and techniques are given in §4.1, §4.2, and §4.3.

[b]The photometry errors are taken to be the formal GALFIT errors, or the statistical errors from photon noise in the photometry aperture, added in quadrature to the rms photometric calibration errors for the SDSS DR5 (Adelman-McCarthy et al. 2007).

[c]The magnitudes have been corrected for Milky Way extinction, using values from the SDSS DR5 database, which are in turn based on the dust maps of Schlegel et al. (1998). Specifically, the extinction corrections in $gVriz$ are 0.086, 0.070, 0.063, 0.047, and 0.034 mag, respectively, and $E(B-V) = 0.023$.